Journal of King Saud University – Science 33 (2021) 101266

Contents lists available at ScienceDirect

Journal of King Saud University – Science

journal homepage: www.sciencedirect.com

Original article

Petrology of oolitic ironstones of Ashumaysi Formation of Wadi Fatima, western Arabian Shield, Saudi Arabia

Mahmoud A. Galmed [a,b,*], Bassam A. Abuamarah [a], Habes A. Ghrefat [a], Abdullah A. Al-Zahrani [a]

[a] Geology and Geophysics Department, College of Science, King Saud University, Saudi Arabia
[b] Geology Department, Faculty of Science, Cairo University, Giza, Egypt

ARTICLE INFO

Article history:
Received 24 June 2020
Revised 11 November 2020
Accepted 25 November 2020
Available online 03 December 2020

Keywords:
Petrography
Mineralogy
Ironstones
Oolitic
Ashumaysi
Saudi Arabia

ABSTRACT

The present study concerns Oligo–Miocene oolitic ironstones of the Ashumaysi Formation between Jeddah and Makkah in the western part of the Arabian Shield, western Saudi Arabia. The Ashumaysi Formation contains oolitic iron ore as 2–3 m thick beds. The formation is exposed along the western margin of Wadi Ashumaysi. It dips toward the east and unconformably overlies Precambrian rock and conformably underlies a Miocene basalt flow of the Sita Formation.

The Ashumaysi ironstones are mainly hematitic sandstone and oolitic ironstone. The oolitic ironstones vary in color (reddish, brownish, yellowish, or violet). Petrographic analysis indicated that the ironstones are composed of different shapes of ooids (ooliths), pelloids, and rarely pisoids (pisoliths) within ferruginous cement and matrix, which consists of clay minerals with fine to medium grained quartz XRD with EDX analysis of representative samples indicated that hematite, goethite, chamosite, and quartz are the main components of the oolitic ironstone.

The main processes responsible for the formation of these oolitic ironstones are progressive diagenetic dehydration and recrystallization of the amorphous ferrous hydroxides and the formation of oolitic and pisolitic goethite and hematite within different fabrics.

1. Introduction

Phanerozoic sedimentary ironstones generally occur as thin sequences with oolitic textures deposited in shallow marine or nonmarine environments (Young et al., 1989; Taylor, 1992). It is widely believed that the concentric rings that are characteristic of oolites are formed primarily by chemical precipitation (Yoshida et al., 1998). The occurrence of oolitic ironstones commonly corresponds to times of relatively high sea level, when warm and humid climate enabled chemical weathering (Blatt et al., 1980; Gilbert and Park, 1986). However, the process by which oolitic textures form and the timing of hematite crystallization in these rocks is still a matter of conjecture (Maynard, 1983; Young et al., 1989; Kimberley, 1994).

Since the discovery of oolitic hematite beds in the Fatima and Ashumaysi areas, the Ashumaysi Formation, of probable Oligocene age (Cox, 1964), has become the most important sedimentary sequence between Makkah and Jeddah in Saudi Arabia. The Ashumaysi Formation contains two main oolitic iron ore beds varying in thickness from 2 to 3 m thick. The total ore reserves in the district are considered to be ~70 million tons, averaging ~45–48% iron content. Extraction of this iron ore will help diversify the economy of the country, which for the last 20 years has depended on oil as its main source of revenue. The government of Saudi Arabia is planning to build a steel plant in Jeddah and to mine the iron ore in the Ashumaysi Formation. The origin and environment of iron ooids have long been subject to assumptions and conjecture. These are thought to be deposited at a very slow rate as condensate sequences in moderately to very shallow water conditions (Burkhalter, 1995).

The study area (Fig. 1) is a part of the Makkah topographic quadrangle sheet (Moore and Al-Rehaili, 1989), and it is in the southern part of the Hijaz geographic province. A flat, low- lying coastal plain (Tiharnat Al Hijaz) is followed eastward by the rugged

* Corresponding author. Geology and Geophysics Department, College of Science, King Saud University, Saudi Arabia.
E-mail address: mgalmed@ksu.edu.sa (M.A. Galmed).

Peer review under responsibility of King Saud University.

Production and hosting by Elsevier

https://doi.org/10.1016/j.jksus.2020.101266
1018-3647/

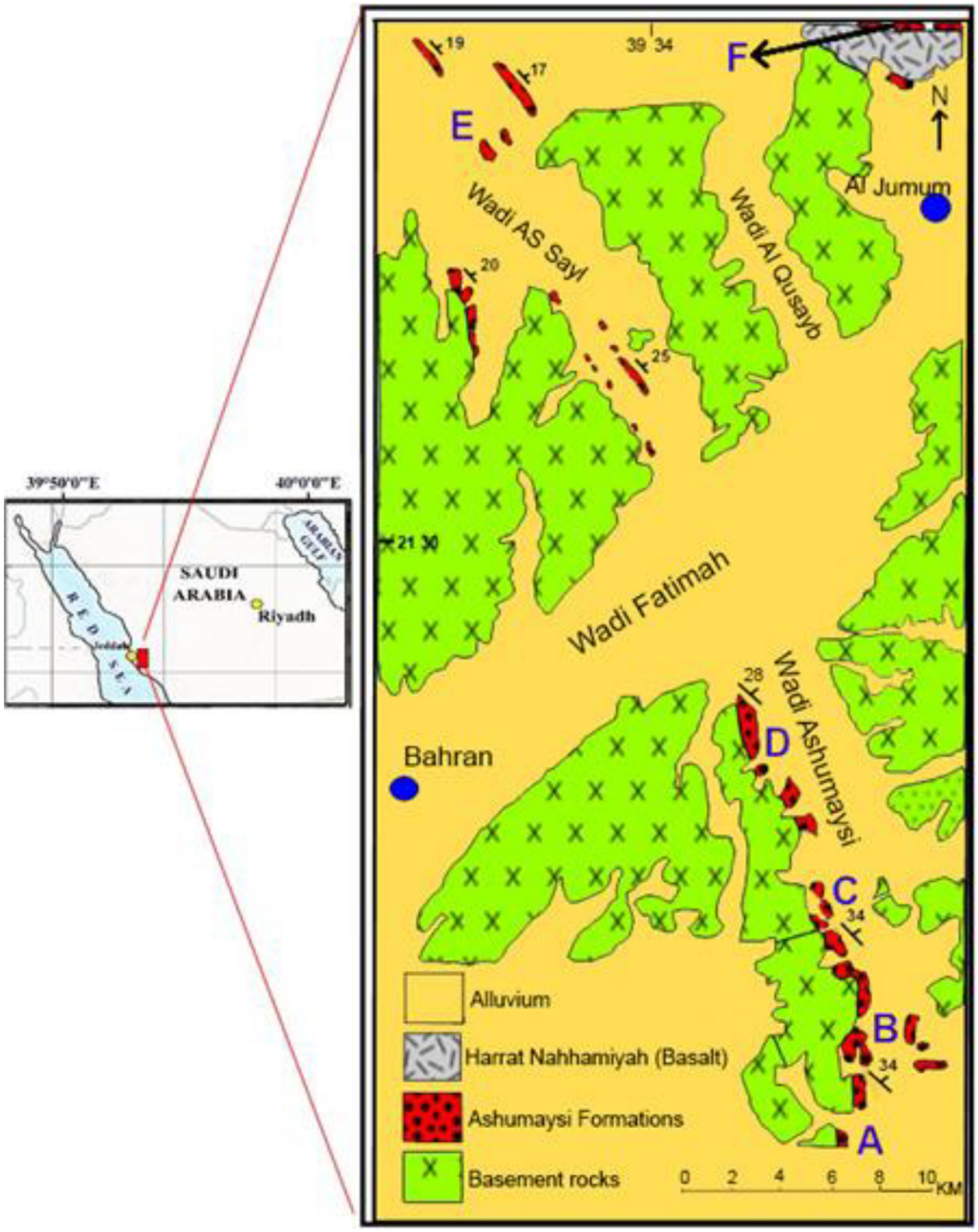

Fig. 1. Location and geologic map of study area, modified after Al-Shanti (1966) and Moore and Al-Rehaili (1989).

Sarawat Mountains, which culminate in a major erosional escarpment that resulted from uplift of the Arabian Shield in association with Red Sea rifting (Moore and Al-Rehaili, 1989). A moderately dissected plateau slopes gently eastward from the edge of the escarpment, which is portrayed toward the east side of the quadrangle. The flat Cenozoic Harrat Rahat lava field (extrusion began at about 10 Ma, Camp and Roobol, 1987) and its erosional remnants occur in the northern part of the area represented by the quadrangle.

The eastward-dipping Ashumaysi Formation, which occupies the Ashumaysi trough, is exposed along the western margin of Wadi Ashumaysi. These exposures tilt toward the northeast with an angle in the range 15°–35°. The formation unconformably overlies Precambrian basement and conformably underlies a basalt flow of the Miocene Sita Formation. Although the basal unconformity is not exposed in this area, the contact with the overlying basalt at the base of the Sita Formation is exposed for a short distance at one locality.

Although the thickness of the Ashumaysi Formation varies in the range ~74–183 m, the section as measured by Al-Shanti (1966) at Wadi Ashumaysi is ~141 m thick. He subdivided it into three parts: a 64 m-thick basal part, a 13.4 m-thick middle part, and a ~64 m-thick upper part. On the basis of fossils from different outcrops of the Ashumaysi Formation in the map area, Cox (1964) concluded that the age of the formation is Oligocene, which is younger than earlier thought (Eocene).

However, Al-Shanti (1966) concluded that the deposition of Ashumaysi Formation occurred under a shallow-water environment with marked transgression and regression of the sea during the deposition of the three different parts. The presence of oolitic

iron-ore beds in the middle part suggests strong wave action. Also, Al-Shanti (1966) concluded that, turbidity and agitation caused alumina-gel and hydrohematite colloids in the water; to attach themselves to nuclei of either silica (in the form of angular quartz grains) or of hematite grains. The stratigraphic setting of the actual oolitic ironstones and their composition, textural maturity, internal sedimentary structures, and lateral facies changes intensified the concentration of their ferruginous ooids. The short-lived, small-scale prograding regimes were terminated during the highly agitated conditions along bar flanks and bar crests during the regressive events (Taj, 2011).

2. Materials and methods

During our field study, we measured and sampled the lithostratigraphic sections. For microscopic examination, we collected a representative set of 70 samples from different lithologies, particularly the oolitic iron ore. We then took corresponding photomicrographs and prepared careful descriptions of the minerals, grains, intergranular relationships and aggregates, and matrix or cements for each sample. We also used X- Ray Diffraction (XRD) analysis to examine 15 samples representing the main lithologies and the oolitic iron ore of the Ashumaysi Formation in the study area. To facilitate accurate mineral identification, the XRD analysis was conducted on powdered bulk samples from various rock types.

We used a high-performance Scanning Electron Microscope (JSM-6380 LA) with a Kevex-Ray unit to reveal textural relationships among the minerals. Running at 0.3–30 kv, the resolution of the unit was 3.0 nm and the magnification was 18–300,000X. Maximum specimen size was 203.2 mm. By also enabling morphological identification of the minerals, this SEM analytical technique afforded accurate mineral identification and was particularly useful for determining the minerals of the oolitic iron ore minerals and the matrix or cement. We prepared 12 representative samples for SEM study; after initial ultrasonic cleaning of the specimens, we coated the fresh surfaces with a gold–palladium alloy. For qualita-

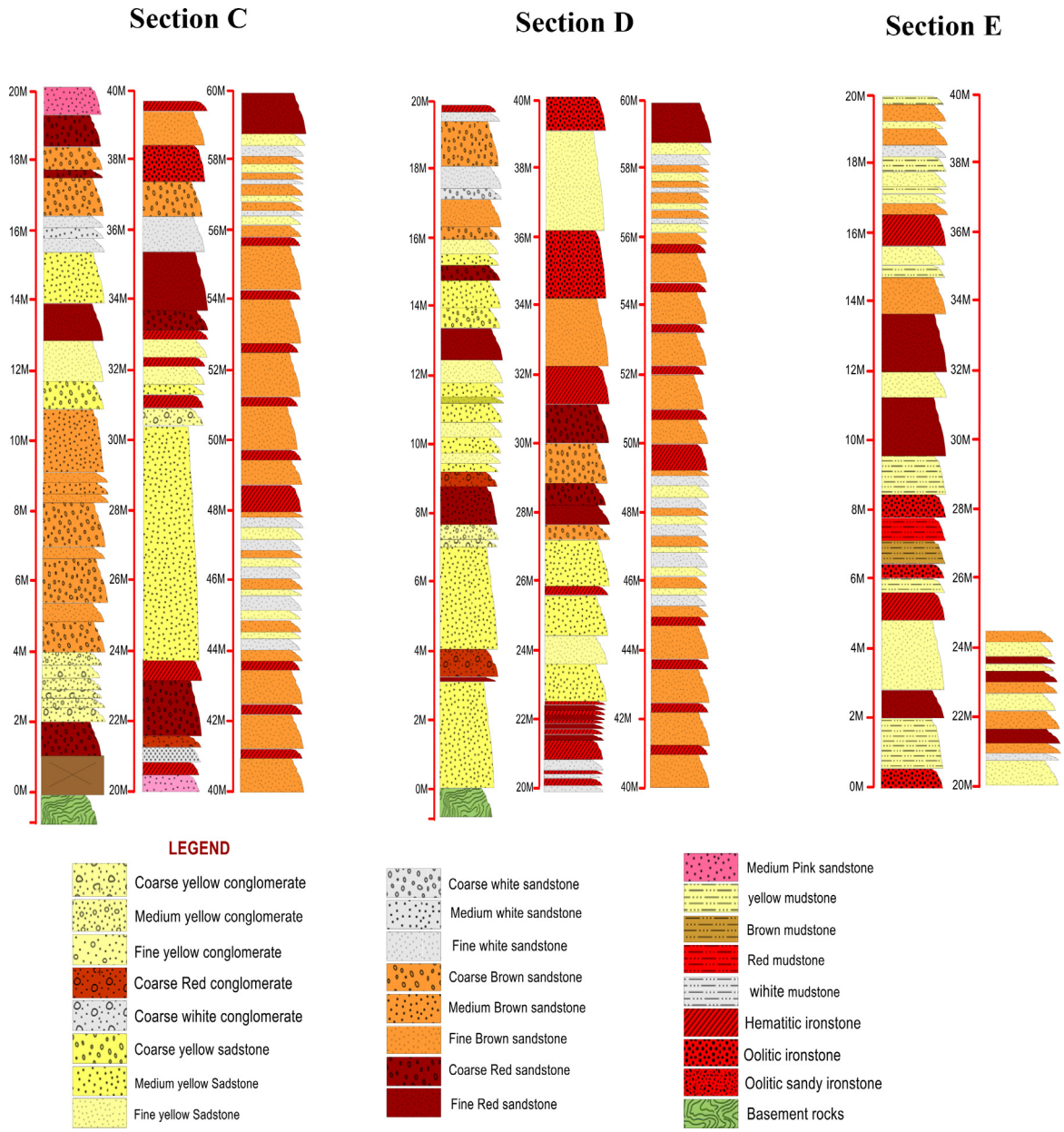

Fig. 2. Lithostratigraphic columnar sections of Ashumaysi Formation at field locations C, D, and E.

tive chemical analysis, we ran EDX analyses. By linking the EDX unit to a data-processing computer (Welton, 1984), we were able to gather all 12 signals simultaneously with error as low as 1%. The obtained spectra were processed by using a Link Analytical Systems AN1000 computer, which interactively corrected for the effects of atomic number and for absorbance and fluorescence factors.

3. Results

3.1. Lithostratigraphy

Generally, the Ashumaysi Formation in the study area is a clastic sedimentary succession that includes intermittent hills rising gently from the valleys along the western banks and rests noncon-

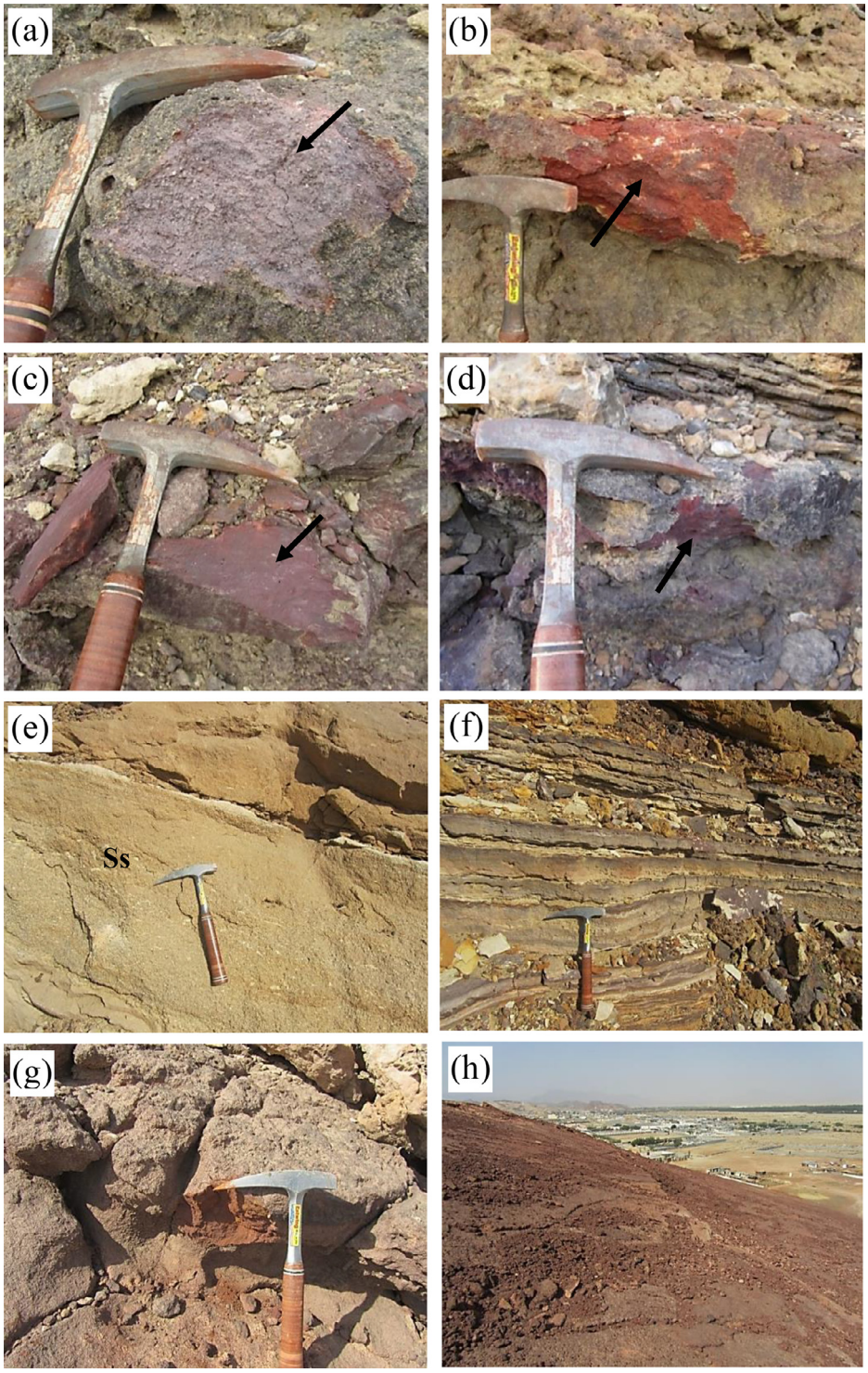

Fig. 3. Field photographs of studied outcrop sections C (a–d) and D (e–h): (a) Oolitic ironstone(arrow). (b) Reddish oolitic ironstone beds (arrow). (c) Reddish-violet oolitic ironstone bed (arrow). (d) Thin, reddish-to-violet oolitic ironstone bed at the upper part of section (arrow). (e) Reddish medium- to coarse-grained sandstone beds (Ss). (f) Alternating sequences of hematitic ironstone, fine-grained sandstone, and white mudstone beds. (g) Two oolitic ironstone beds (in middle part of section). (h) Alternating sequences composed of ferruginous medium- to coarse-grained sandstone (in upper part of section).

formably on crystalline basement rock (Fig. 1). These small, dark-brown to black isolated hills that expose the formation are controlled mainly by northwest-oriented faults flanking Wadi Ashumaysi. We measured six stratigraphic sections (A–F in Fig. 1), varying in thickness (height) within ~20–65 m. The lowermost sections of the studied succession are not completely exposed but are represented by the appearance of pebbles and cobbles of quartz grains. This represents a very proximal facies in the lowermost part of the sequence as a result of the high magnitude of the northwest-trending faults alongside the wadi. The following paragraphs describe three sections that are representative of the main outcropping lithostratigraphic units.

In studied section C, the Ashumaysi Formation is ~60 m thick and is nonconformable with the underlying basement rock (Fig. 2). The lower part of the formation is covered mostly by a ~10-m-thick of fragmented slumped rocks. Bedded and alternating conglomerate and medium- to fine-grained sandstone nonconformably overlie the erosional surface of the crystalline basement rock. Ferruginous sandstone beds top the conglomerate-and-sandstone layers. These are overlain by a deep-red 1.5-m-thick oolitic ironstone beds (Fig. 3a), which gradually change from reddish to reddish violet (Fig. 3b–3d) and in some places midsection occur as reddish to yellowish sandy oolitic ironstone. The upper part of the section is composed of rhythmically alternating red to yellowish bedded mudstone. At the top of the section, siltstone and red to yellowish medium- to fine-grained sandstone alternate with mudstone. The studied section is capped with a thin, reddish oolitic ironstone bed.

In studied section D, the Ashumaysi Formation is also ~60 m thick and is nonconformable with the underlying basement rock (Fig. 2). The section begins at the base with several depositional cycles composed of coarse- to fine-grained sandstone with some conglomeratic layers. Thin, ferruginous sandstone layers and very fine-grained reddish sandstone with some white, fine-grained sandstone alternate to form distinct depositional cycles (Fig. 3e and 3f). Two oolitic ironstone beds with different thicknesses overlie these cycles in the middle part (Fig. 3g). Another oolitic ironstone bed is in the upper part of the studied section (Fig. 3h).

The third studied section, E, is ~25 m thick and is in the northern part of the study area (Fig. 2). A 0.5-m-thick oolitic ironstone bed is the lowest exposed unit in the section (Fig. 4a). Hard reddish mudstone layers overlie this oolitic ironstone bed (Fig. 4b). The massive mudstone is overlain by medium- to coarse-grained sandstone exhibiting graded bedding. The oolitic ironstone varies in but is mostly ~40 cm thick. The upper part of the section is composed of thin, successive, multicolored reddish fine-grained sandstone beds (Fig. 4c) overlain by red ~15-cm-thick oolitic ironstone. A reddish fine- to medium-grained hematitic sandstone bed in the upper part of the section (Fig. 4d) is overlain by upward-thinning cyclic beds, in which each cycle begins with a lower silty mudstone or siltstone that grades upward into a ferruginous muddy and silty massive ironstone (oolitic ironstone) bed.

3.2. Petrography

The Ashumaysi ironstones are mainly hematitic sandstone and oolitic ironstone. The oolitic ironstone rock samples are vary in color, reddish, brownish, yellowish, and violet colors. They are composed of ooids (ooliths), pelloids, and rarely pisoids (pisoliths) within ferruginous cement and matrix. The matrix consists of clay minerals and fine- to medium-grained quartz.

The ooids vary in shape from rounded (spheroidal) to elliptical. Each consists of concentric layers of varying composition around a core. These layers consist mainly of hematite, goethite, and chamosite. The cores are mainly massive hematite and goethite, quartz grains, and broken ooids, or they may be empty (or undefined). The studied oolitic sandstone of the Ashumaysi Formation consists of fine- to medium-grained, angular to subrounded quartz sand cemented by hematitic materials. Ultimately, the embayed quartz is the result of the corrosion of the quartz grains by the hematitic

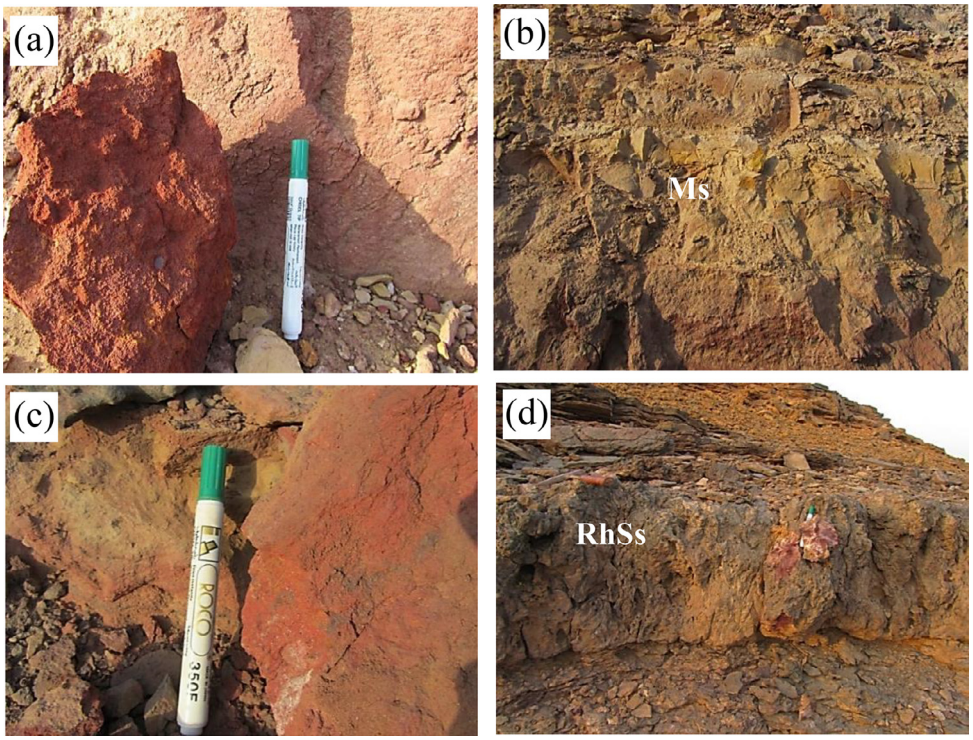

Fig. 4. Field photographs of studied outcrop section E: (a) Two ~0.5-m-thick oolitic ironstone beds. (b) Hard (massive) reddish mudstone layer (Ms). (c) Reddish hematitic sandstone bed (RhSs). (d) Reddish hematitic sandstone bed (in upper part of section).

domains that gradually formed (Fig. 5a). The studied oolitic ironstone in some thin sections have well-laminated grains (Fig. 5b).

Most of the studied ironstone oolites are spheroidal (well rounded) with minor or subordinate elliptical types (Fig. 5a). The ooids are composed of outer or concentric layers of hematite and goethite, which are poorly distinguished in some ooids. Most of the oolites are of single type grain with some showing composite grains (Fig. 5c). Some elliptical or ovoidal ooids may not have cores or may have concentric layers lacking cortices (Fig. 5d). The spheroidal or elliptical ooids of the Ashumaysi ironstone have different

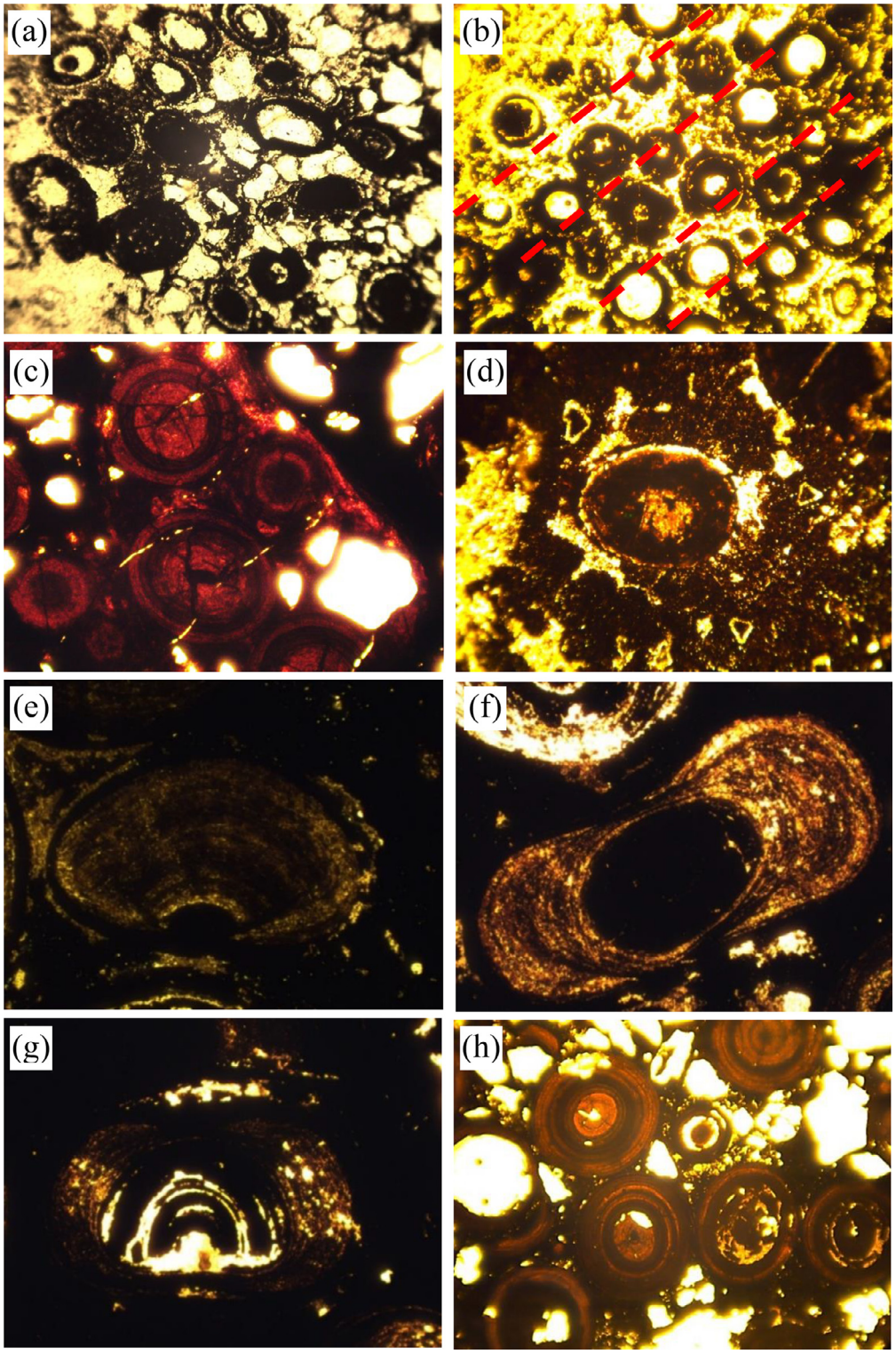

Fig. 5. Photomicrographs of oolitic ironstone of Ashumaysi Formation: (a) Oolitic sandstone showing ultimate stages of corrosion of quartz grains with advancing hematitic domains (PPL, 10x). (b) Well-laminated, rounded oolitic ironstone (PPL, 10x). (c) Composite grains consisting of several ooids (PPL, 10x). (d) Ovoidal ooid (lacking cortex) in hematitic matrix (PPL, 10x). (e) Ooid grain with eccentric core (PPL, 10x). (f) Fusiform ooid grain (PPL, 10x). (g) Fragmented ooid grain with incomplete cortex (PPL, 10x). (h) Well-rounded ooids with well-defined cortex (XPL, 10x).

shapes and compositions. Some have well-defined cortices and different core compositions and shapes. Eccentric cores and thick cortices are seen in some thin sections (Fig. 5e). Other ooids show fusiform shape due to different pressures and winnowing effects; others have complete or incomplete cortices around fragmented ooids (Fig. 5f).

Some spheroidal or egg-shaped ooids were subjected to deformation and show radial shrinkage fractures and empty cores (Fig. 5g). Well-rounded ooids and well-defined cortices of different ooid sizes and various core compositions have been observed within matrices composed of fine- to medium-grained quartz and hematite–goethite cement (Fig. 5h). Some of these ooids, particularly the elliptical ones, have asymmetric cortices.

Well-defined cortices with thick laminae including white chamositic layers were observed in some samples of well-rounded ooids; some show fragmented hematitic cores and others have empty cores and hematite–goethite cement (Fig. 6a and 6b). Some of the ooids are broken owing to compaction. In some of the elliptical ooids, the cores are composed of quartz grains (Fig. 6c) with hematite iron cores; others have undefined or empty cores (Fig. 6d).

The ooids of the Ashumaysi ironstone were subjected to late diagenesis represented by fragmentation and dissolution. In many samples, we found evidence of dissolved ooids, which were probably due to physicochemical conditions that led to the etching and digestion or dissolution of the ooids into the matrix (Fig. 6e). The progress of hematitization and corrosion led to the transformation of the ironstone oolite grains in the matrix, resulting in extensive areas of hematite cement. Some ooids are completely dissolved and have become cementing materials, whereas others are found as relics or remnants (Fig. 6f).

Diagenetic processes played important roles in the evolution of the oolitic ironstone. The diagenetic recrystallization and dehydration of the precursor amorphous iron-bearing clays are closely associated with the progressive formation of ferrous hydroxides, goethite, and hematite in successive stages of water loss. These processes began with the formation of honey-colored clays stained by ferrous hydroxides.

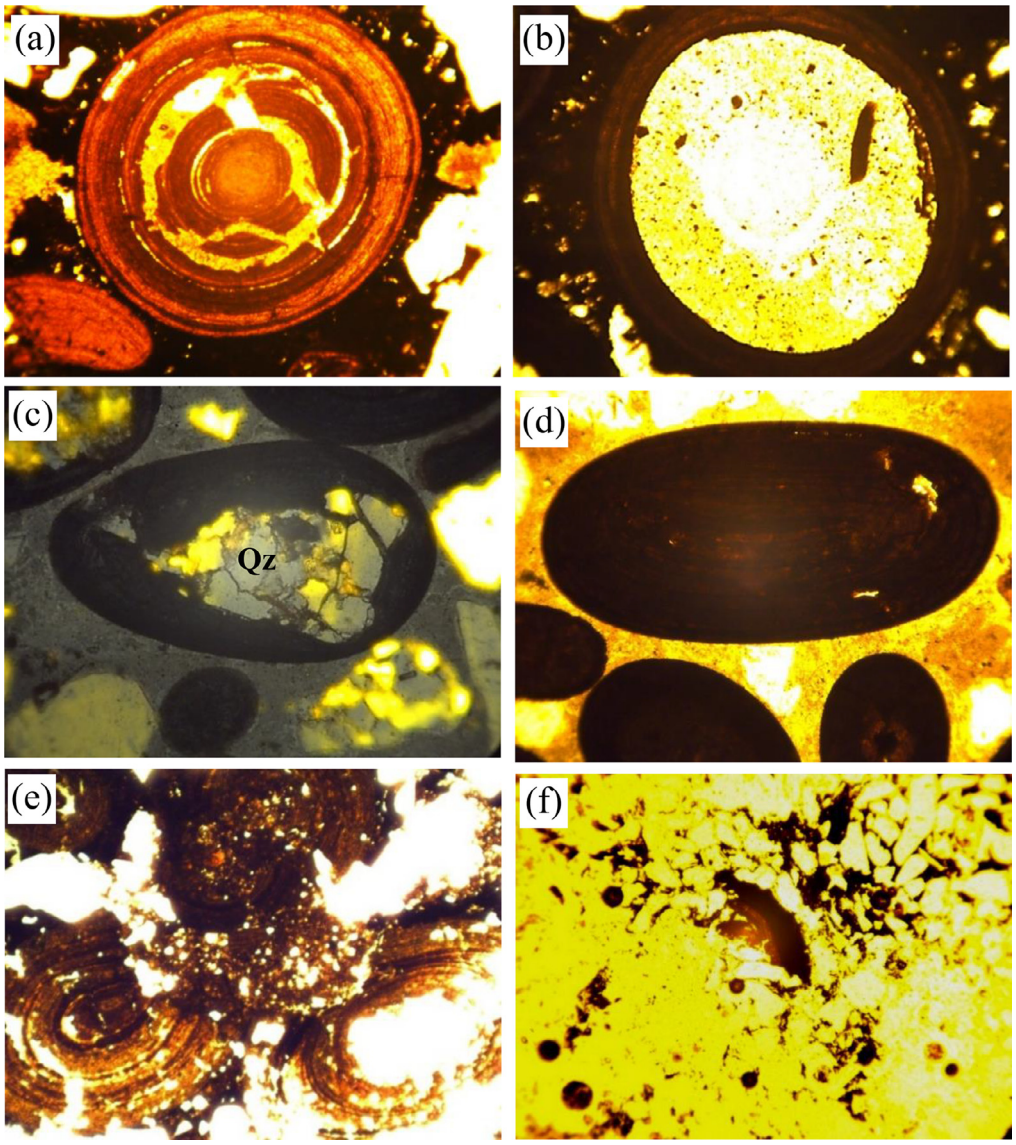

Fig. 6. Photomicrographs of oolitic ironstone of Ashumaysi Formation: (a) Well-rounded ooid with well-defined cortex, showing slight fragmentation (PPL, 25x). (b) Ooid with well-defined cortex without core (PPL, 25x). (c) Elliptical or ovoidal oolitic iron grain with core composed of quartz grains (Qz) (XPL, 10x). (d) Elliptical ooid without core (PPL, 25x). (e) Progress of hematitization and corrosion that led to transformation of oolitic iron grains into matrix as a result of widespread hematite-cement formation (PPL, 10x). (f) Ooid remnant from transformation and dissolution processes (PPL, 10x).

3.3. Mineralogy

XRD analysis of representative samples indicated that the main compositions of the oolitic ironstone are hematite, goethite, chamosite, and quartz (Fig. 7). We obtained SEM images and EDX spectra of the hematite and chamosite in the studied oolitic iron ore (Fig. 8), which together indicated that the bright parts in the SEM images are hematite, clearly the main mineral in the Ashumaysi oolitic iron ore. The hematite exists in two forms: as very fine grains in concentric oolitic layers (Fig. 8a–8d) and as larger grains in the spaces between the aggregated ooids.

Goethite we found to occur in various forms-as concentric monomineralic layers in some ooliths or alternating with hematite in other samples; in massive form and disseminated in the matrix; in ooid cores, with a spongy appearance; and/or as colloidal traces. The goethite was readily distinguished by XRD analysis (Fig. 7). Chamosite, a ferrous aluminous silicate (Chemically, it resembles the iron-rich chlorite), contains regularly alternating layers with tetrahedral and tri-octahedral components. (Its 2:1 layer structure is similar to that of mica, with a basal spacing of 14 Å.) Its general composition is $(Mg,Fe,Al)_6(Al,Si)_4O_{10}(OH)_8$, where iron is the main component,

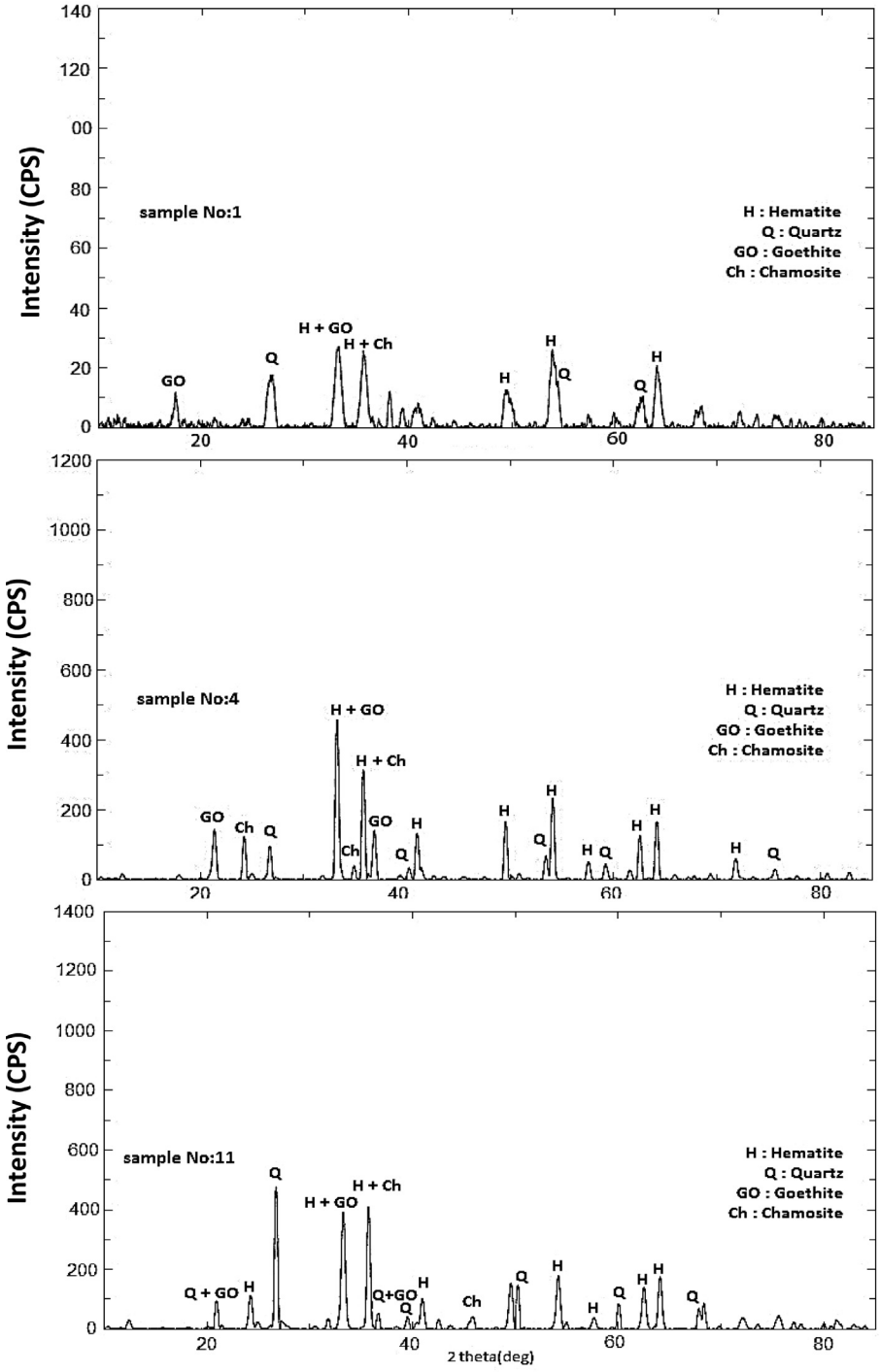

Fig. 7. XRD pattern for representative oolitic ironstone samples of Ashumaysi Formation.

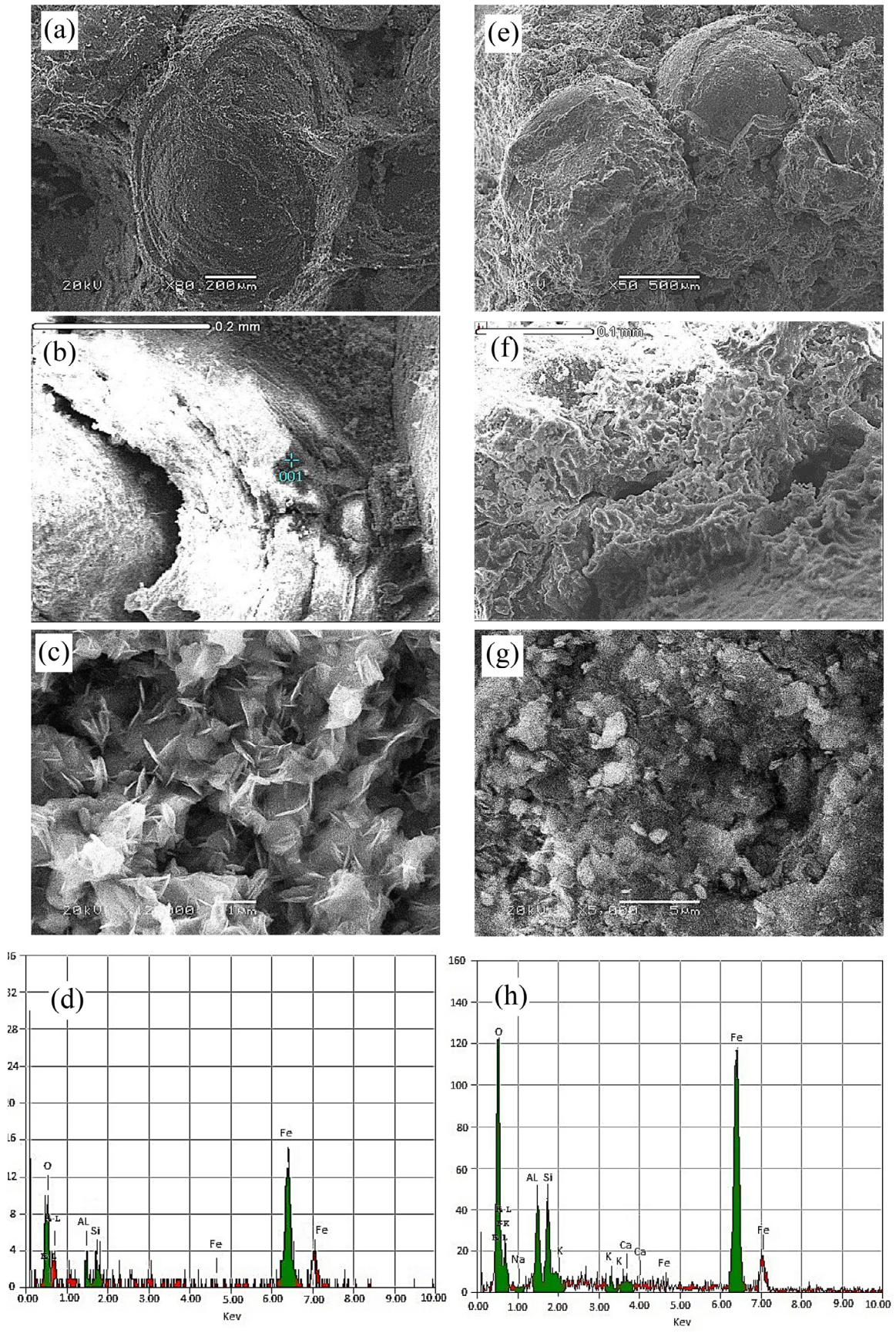

Fig. 8. SEM and EDX analytical results. (a) Ovoidal iron ooid. (b) Ooid microtextures showing concentric layers. (c) Hematitic composition of cortex. (d) Results of EDX analysis representing hematitic composition of cortex. (e) Iron ooids and cementing materials. (f) Microtextures of cortex and cementing materials. (g) Chamositic flecks of ooid and cementing materials. (h) Results of EDX analysis.

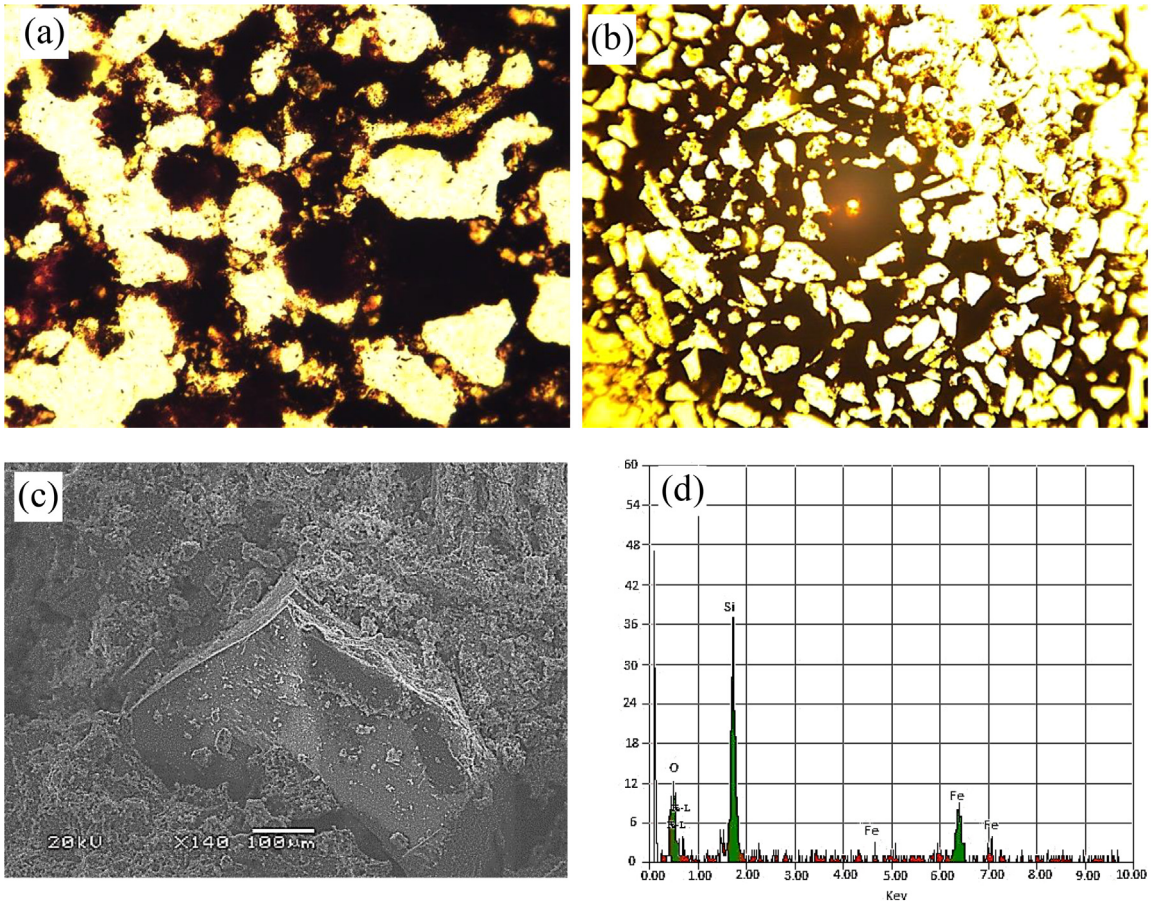

Fig. 9. PPL, SEM, and EDX analytical results. (a) Rounded and empty ooids with pelloids within hematitic sandstone (PPL, 25x). (b) Hematitic fine-grained sandstone and pelletal grains within highly angular and embayed quartz (PPL, 10x). (c) SEM image of detrital quartz grain in groundmass (matrix). (d) EDX analysis of matrix and spot analysis of quartz grain.

aluminum is in lower proportion, and magnesium and silica are slightly higher in proportion than the aluminum.

The chamosite ooids commonly contain concentric layers of oxidized materials representing interludes of higher redox potential in the bottom environment during accumulation. As expected, the Al_2O_3 content is higher than in most other types of ironstones, and thus the chamosite can be considered as largely a product of sea-bottom reactions between ferrous iron in solution and detrital clay particles (James, 1966; Bhattacharyya, 1980; Bhattacharyya and Kakimoto, 1982; Bhattacharyya, 1983, 1989; Rude and Aller, 1989). However, the replacement of clastic material by chamosite indicates that the formation process was not simply clay diagenesis. The SEM images and EDX spectra for representative samples (Fig. 8e–h) show chamosite flecks with the hematite–goethite minerals in both the concentric layers and the groundmass.

Quartz in the Ashumaysi oolitic iron ore is granular (detrital) in form and is found inside the ooids and in the spaces between the aggregated ooids (Fig. 9a–d). Although its particle size ranges from medium-grained to very fine sand, the majority of particles are commonly of fine sand. The granular quartz exists (Fig. 9c and d). Because the quartz does not appear as oolitic layers but instead as nuclei associated with the iron oxides, the quartz in the Ashumaysi oolitic iron ore apparently is easily liberated from the hematite to separate out the iron minerals.

4. Discussion

Ferretti (2005) considered that the origin and formation of the oolitic ironstones were still under discussion but were agreed to be within the context of low-energy (e.g., Gygi, 1981) or turbulent (e.g., Hallam, 1975) hydrodynamic systems. These have been thought to have been related (e.g., Hallam and Bradshaw, 1979; Van Houten and Purucker, 1984; Bayer et al., 1985; McGhee and Bayer, 1985; Teyssen, 1989; Young, 1989a) or unrelated (e.g., James and Van Houten, 1979) to sea-level fluctuations. Where sea-level changes have been considered to play a role, iron ooids have been variously interpreted as having formed at sea-level lowstands (e.g., Dreesen, 1989; Madon, 1992), during transgressions (e.g., Young, 1989b; Chan, 1992; Burkhalter, 1995; Taylor et al., 2002), or at maximum-flooding surfaces (e.g., Young, 1992). Heikoop et al. (1996) reported modern primary iron ooids in reef areas characterized by hydrothermal-water venting.

The studied oolitic ironstones were initially formed of fine-grained hematite, which is commonly distributed in the cortices of the ooids. The ooids rolled over in agitated waters and acquired successive concentric layers by the enveloping precipitation of colloidal hydrohematite and alumina gel. The red ferruginous beds of the Precambrian Fatima Series in the area are considered to have been the main source of hematite forming the oolites (Al-Shanti, 1966). Conversion of Fe-rich materials that were initially contained in unconsolidated ooids, the hematite (Fe_2O_3) likely formed by secondary diagenetic processes. The hydrated ferric oxide precursor, such as an amorphous FeO–OH or goethite, was considered to have been the main source of hematite in sedimentary rocks that diagenetically formed by an aging process that involved dehydration (Tucker, 1991).

After the formation and consolidation of the initial ooids, the material was converted to hematite–chamosite ooids during diage-

nesis. Although the formation process of chamosite [$(Mg,Fe)_3Fe_3(Si_3Al)O_{10}(OH)_8$] is poorly understood, it is assumed to precipitate in environments that fluctuate from oxic to anoxic conditions without sulfide activity (Kimberley, 1979; Tucker, 1991).

The color conversion of in-situ peloids from reddish-brown to black reflects the final stages of dehydration and recrystallization of the ferrous hydroxides, during which oolitization occurred (by the tangential growth of the ferrous hydroxides) and pseudo-ooids formed.

5. Conclusions

On the basis of data obtained from field observations and petrographic and mineralogical studies of the Ashumaysi Formation, we concluded the following:

- The oolitic ironstones of the Ashumaysi Formation between Jeddah and Makkah are enclosed mainly within the middle part of the Oligo–Miocene siliciclastic succession of the western part of the Arabian Shield, western Saudi Arabia.
- The complete hematitization of the formed ferrous hydroxides laminae and the formation of black peloids with very faint oolitic structure occurred during the final stages of dehydration and recrystallization.
- The amorphous ferrous hydroxides were diagenetically recrystallized into goethite and hematite during prolonged stages of advanced hematitization.
- The enveloping chamosite and hematite layers show that the two minerals are of contemporaneous origin, although the hematite also has replaced chamosite.
- The ooids were transformed and dissolved and the hematitic–goethitic cement formed by late diagenetic processes.
- Replacements occurred diagenetically while the sediments were still unconsolidated, and apparently no significant amounts of iron have been added since sedimentation ceased.

Conflict of interest

There is no any conflict and the authors extend their appreciation to the Deanship of Scientific Research at King Saud University for funding this work through research group No (RG-1439-037).

Acknowledgement

The author would like to extend his appreciation and gratefulness to the Deanship of the Scientific Research and RSSU at King Saud University for funding and supporting this work via Research Group Number RG-1439-037.

References

Al-Shanti, A. 1966. Oolitic iron ore deposits in Wadi Fatima between Jeddah and Mecca, Saudi Arabia. Saudi Arabian Directorate General of Mineral Resources, Bulletin 2, 51p.

Bayer, A., Altheimer, E., Deutschle, W., 1985. Environmental evolution in shallow epicontinental seas: Sedimentary cycles and bed formation. In: Bayer, U., Seilacher, A. (Eds.), Sedimentary and Evolutionary Cycles. Lecture Notes in Earth Sciences 1, pp. 347–381.

Bhattacharyya, D.P. 1980. Sedimentology of the Late Cretaceous Nubia Formation at Aswan, Southeast Egypt, and Origin of the associated ironstones. Ph.D. Thesis, Princeton University, 122p.

Bhattacharyya, D.P., 1983. Origin of berthierine in ironstones. Clays. Clay. Miner. 31, 173–182.

Bhattacharyya, D.P., 1989. Concentrated and lean oolites examples from the Nubia Formation at Aswan, Egypt and significance of the oolite types in ironstone genesis Special Publication 46. In: Young, T.P., Taylor, W.E.G. (Eds.), Phanerozoic Ironstones. Geol Soc, London, pp. 93–103.

Bhattacharyya, D.P., Kakimoto, P.K., 1982. Origin of ferriferous ooids: a SEM study of ironstone ooids and bauxite pisoids. J. Sed. Pet. 52, 849–857.

Blatt, H., Middleton, G., Murray, R., 1980. Origin of Sedimentary Rocks. Prentice-Hall, Englewood Cliffs, NJ.

Burkhalter, R.M., 1995. Ooidal ironstone and ferruginous microbialites: origin and relation to sequence stratigraphy (Aalenian and Bajocian, Swiss Jura Mountains). Sedimentology 42, 57–75.

Camp, V.E., Roobol, M.J. 1987. Geologic map of the Cenozoic Harrat Rahat lava field, Kingdom of Saudi Arabia; Saudi Arabia Deputy Ministry for Mineral Resources Geoscience Map (with text), scale 1:250,000, Open-file Report DGMR-OF-07-9, 101 p.

Chan, M., 1992. Oolitic ironstone in the Cretaceous Western Interior Seaway, East-Central Utah. J. Sediment. Petrolo. 62, 693–705.

Cox, L.R. 1964. Fossils from Shumaysi Formation. Unpublished Report.

Dreesen, R., 1989. Oolitic ironstones as event-stratigraphical marker beds within the Upper Devonian of the Ardenno-Rhenish Massif. In: Young, T.P., Taylor, W.E.G. (Eds.), Phanerozoic Ironstones. Mineralium Deposita, pp. 65–78.

Ferretti, A., 2005. Ooidal ironstones and laminated ferruginous deposits from the Silurian of the Carnic Alps, Austria. Bollettino Della Società Paleontologica Italiana 4, 263–278.

Gilbert, J.M., Park Jr., C.F., 1986. The Geology of Ore Deposits. W. H Freeman, New York.

Gygi, R.A., 1981. Oolitic iron formations: marine or not marine? Eclogae Geologicae Helvetiae 74, 233–254.

Hallam, A., 1975. Jurassic Environments. Cambridge University Press, Cambridge, United Kingdom.

Hallam, A., Bradshaw, M.J., 1979. Bituminous shales and oolitic ironstones as indicators of transgressions and regressions. J. Geol. Soc. Lond. 136, 157–164.

Heikoop, J.M., Tsujita, C.J., Risk, M.J., Tomascik, T., Mah, A.J., 1996. Modern iron ooids from a shallow marine volcanic setting: Mahengetang, Indonesia. Geology 24, 759–762.

James, H.L. 1966. Chemistry of the iron-rich sedimentary rocks. In Data of Geochemistry, U.S. Geological Survey Professional Paper 440-W. 60 pp.

James, H.E., Van Houten, F.B., 1979. Miocene goethitic and chamositic oolites, northeastern Colombia. Sedimentology 26, 125–133.

Kimberley, M.M., 1979. Origin of oolitic iron formations. J. Sediment. Res. 49 (1), 111–131.

Kimberley, M.M., 1994. Debate about ironstone: Has solute supply been surficial weathering, hydrothermal convection, or exhalation of deep fluids? Terra Nova 6, 116–132.

Madon, M.B.H., 1992. Depositional setting and origin of berthierine oolitic ironstones in the Lower Miocene Terengganu Shale, Tenggol Arch, Offshore Peninsular Malaya. J. Sediment. Petrol. 62, 899–916.

Maynard, J.B., 1983. Geochemistry of sedimentary ore deposits. Springer-Verlag, New York.

McGhee Jr, G.R., Bayer, U., 1985. The local signature of sea-level changes. In: Bayer, U., Seilacher, A. (Eds.), Sedimentary and Evolutionary Cycles. Lecture Notes in Earth Sciences 1, pp. 98–112.

Moore, T.A., Al-Rehaili, M.H. 1989. Geologic Map of the Makkah Quadrangle, Sheet 21D, Kingdom of Saudi Arabia, Ministry of Petroleum and Mineral Resources, Directorate General of Mineral Resources Geoscience Map GM-107C, 1:250,000 Scale.

Rude, P.D., Aller, R.C., 1989. Early diagenetic alteration of lateritic particle coatings in Amazon continental shelf sediments. J. Sed. Pet. 59, 704–716.

Taj, R.J., 2011. Stratigraphic setting, facies types and depositional environments of Haddat Ash Sham Ironstones, Western Arabian Shield, Saudi Arabia. Asian Trans. Basic Appl. Sci. 1, 1–25.

Taylor, K.G., 1992. Non-marine oolitic ironstones in the Lower Cretaceous Wealden sediments of southeast England. Geol. Mag. 129, 349–358.

Taylor, K.G., Simo, J.A., Yocum, D., Leckie, D.A., 2002. Stratigraphic significance of ooidal ironstones from the Cretaceous Western Interior Seaway: The Peace River Formation, Alberta, Canada, and the Castlegate Sandstone, Utah, U.S.A. J. Sediment. Res. 72, 316–327.

Teyssen, T., 1989. A depositional model for the Liassic Minette ironstones (Luxemburg and France), in comparison with other Phanerozoic ooidal ironstones. In: Young, T.P., Taylor, W.E.G. (Eds.), Phanerozoic Ironstones, pp. 79–92. Geological Society Special Publication 46.

Tucker, M.E., 1991. Sedimentary Petrology. Blackwell Science Publishers, London.

Van Houten, F.B., Purucker, M.E., 1984. Glauconitic peloids and chamositic ooids – favorable factors, constraints, and problems. Earth-Sci. Rev. 20, 211–243.

Welton, J.E., 1984. SEM Petrology Atlas. American Association of Petroleum Geologists, Tulsa.

Yoshida, M., Khan, I.H., Ahmad, M.N., 1998. Remanent magnetization of oolitic ironstone beds, Hazara area, Lesser Himalayan thrust zone, Northern Pakistan: Its acquisition, timing, and paleoenvironmental implications. Earth Planets Space 50, 733–744.

Young, T.P., 1989a. Phanerozoic ironstones: An introduction and review. In: Young, T.P., Taylor, W.E.G. (Eds.), Phanerozoic Ironstones, pp. 9–25. Geological Society Special Publication 46.

Young, T.P., 1989b. Eustatically controlled ooidal ironstone deposition: facies relationships of the Ordovician open-shelf ironstones of Western Europe. In: Young, T.P., Taylor, W.E.G. (Eds.), Phanerozoic Ironstones, pp. 51–63. Geological Society Special Publication 46.

Young, T.P., 1992. Ooidal ironstones from Ordovician Gondwana: A review. Palaeogeogr. Palaeoclimatol. Palaeoecol. 99, 321–347.

Young, T.P., Taylor, W.E.G. (Eds.), 1989. Phanerozoic Ironstones. Geological Society, LondonLondon, pp. 1–251. Special Publications 46.